Available online at www.sciencedirect.com
ScienceDirect
Trans. Nonferrous Met. Soc. China 35(2025) 2683−2698
Transactions of Nonferrous Metals Society of China
www.tnmsc.cn

Synthesis and performance enhancement mechanisms of Ni−Co−C alloy coatings

Yi-zhe DU[1], Zhen-yao CHEN[1], Hua-mei DUAN[1], Mu-jun LONG[1,2], Deng-fu CHEN[1]

1. Laboratory of Materials and Metallurgy, College of Materials Science and Engineering, Chongqing University, Chongqing 400044, China;
2. National Key Laboratory of Advanced Casting Technologies, Chongqing University, Chongqing 400044, China

Received 4 January 2024; accepted 28 June 2024

Abstract: Ni−Co−C alloy coatings with exceptional properties were fabricated via electrodeposition using an ammonium oxalate−ammonium citrate system. The optimized coatings exhibited dense crystallization with a distinct granular surface, where large particles were covered with nanoscale clusters. Additionally, C atoms primarily existed within the coatings as a solid solution, maintaining the FCC structures. Compared to binary Ni−Co coatings, the Ni−Co−C alloy coatings exhibited significantly improved hardness, wear resistance, and adhesion strength, which could be attributed to the potential strengthening effect of the C atoms. Specifically, the introduction of C atoms optimized the local charge density and electron distribution in the alloy, transforming local weak ionic bonds into strong covalent interactions, thereby enhancing the bonding capability between the corresponding atoms in the NiCo bulk.

Key words: Ni−Co−C alloy coatings; electrodeposition; wear resistance; electronic properties; strengthening mechanisms

1 Introduction

Ni−Co alloys are highly promising materials in the field of materials science and engineering due to their overall performance, including mechanical, magnetic, and catalytic properties [1,2]. In the field of metallurgical continuous casting, Ni−Co alloys have been widely employed as surface coatings for molds, playing a crucial role in enhancing key properties such as wear resistance of molds. In the development of mold coatings, there has been a transition from single metals (pure Cr, pure Ni, etc.) to binary alloys (Ni−Fe, Ni−Co, etc.). The emergence of Ni−Co alloy coatings has somewhat addressed issues such as low stability and poor adhesion in earlier generations of coatings, several challenges, including low hardness and poor wear resistance still persist. Currently, there is an urgent need to develop coatings with superior performance to meet the increasingly stringent quality requirements of continuous casting billets.

Various methods exist to strengthen alloys, among which alloying with foreign elements has proven to be an effective strategy [3,4]. Currently, research has explored the addition of metallic elements such as W, Cr, and Fe to enhance the mechanical properties of Ni−Co alloys [5−7]. In addition, the strengthening effect of adding nonmetallic elements has been proven to be equally significant, especially for typical interstitial

Corresponding author: Deng-fu CHEN, Tel: +86-13658333267, E-mail: chendfu@cqu.edu.cn;
Mu-jun LONG, Tel: +86-13594318151, E-mail: longmujun@cqu.edu.cn
https://doi.org/10.1016/S1003-6326(25)66840-3

elements, as they have the potential to enhance alloy performance through mechanisms such as solid solution strengthening, grain refinement, and second-phase precipitation [8]. Among these, carbon (C), as the most common interstitial element in steel, has demonstrated exceptional strengthening capabilities. In the austenitic phase, C exhibits significant solubility, inducing lattice distortions that hinder dislocation slip. Furthermore, C can effectively anchor dislocations by forming numerous dispersed carbides at the grain boundaries and within the grains, thereby increasing the hardness and strength of the steel [9].

Moreover, there is currently widespread attention on the reinforcing function of C element in various alloys, particularly in high-entropy alloys. For example, research by WANG and BAKER [10] indicated that the addition of C significantly enhanced the yield strength of the FeNiMnAlCr high-entropy alloy, improved the work hardening rate and ductility, and achieved a harmonious balance between strength and plasticity. In addition, SHANG et al [11] found that C can be completely dissolved in NiCoCr high-entropy alloys. This process simultaneously provides interstitial strengthening by increasing the local stacking fault energy, delaying the occurrence of twinning, and reducing the twin layer thickness, thereby favorably affecting the alloy's overall mechanical properties. Similarly, CHEN et al [12] proposed that the mechanical properties of the FeMnNiCr high-entropy alloy reached optimal levels when the C content was 3.3 wt.%. This enhancement was attributed to the hindering effect of C atoms on dislocations, which promoted the formation of numerous deformation twins. The transition from the original dislocation slips deformation mechanism to twin deformation effectively enhanced the mechanical properties of the alloys. Furthermore, C was demonstrated to induce the precipitation of ordered C_xM_y-type carbides in various alloys, exerting a pinning effect at grain boundaries while also regulating the alloy's overall performance [13]. However, experimental studies on the addition of interstitial atoms in Ni−Co coatings have not been reported. Based on existing research, the introduction of C is expected to further enhance the overall performance of Ni−Co alloys, making them promising new-generation coating materials.

Among various surface treatment techniques, electrodeposition has emerged as a primary method for preparing mold coatings due to its mature and facile process, high cost-effectiveness, and superior product quality. However, the electrodeposition of Ni−Co−C alloy coatings faces several challenges, such as the determination of the carbon source and effective coordination agents. Furthermore, this preparation process warrants further exploration and study.

To further improve the service life of the molds, in this study, we conducted a series of screening and optimization studies on the deposition solution and electrodeposition process. We successfully produced high-performance Ni−Co−C alloy coatings and performed detailed characterization and analysis of the coating composition, morphology, structure, and properties. Moreover, using first-principles calculations, we elucidated the strengthening mechanism introduced by carbon atoms at the microscopic level of atomic bonding and electron distribution. These findings provide a foundation for the development and application of a new generation of high-performance Ni−Co−C alloy coatings.

2 Experimental and calculation method

2.1 Coating preparation

The Ni−Co−C alloy coatings were prepared on the surface of the copper alloy matrix via electro-deposition. The detailed experimental procedures and parameters are listed in S1 of the Supplementary Materials (SM).

2.2 Characterization methods

The morphology of the coatings was characterized using a field emission scanning electron microscope (SEM, JSM−7800F). Additionally, an electron probe microanalyzer (EPMA, model number JXA−8530 Plus) was used to obtain a quantitative analysis of the coating's composition. The crystal structure of the coatings was determined by X-ray diffraction (XRD), employing a copper target, using continuous scanning mode with a step size of 0.02° and a scanning time of 30 min. The chemical composition

and elemental oxidation states on the coating surface were examined using X-ray photoelectron spectroscopy (XPS, Thermo Scientific K-Alpha instrument). Charge correction was conducted using the binding energy of C1s (284.8 eV). Scans were performed using an Al K_α X-ray source, and the spot size was set as 400 μm.

2.3 Performance testing

The hardness of the coatings was measured using an automated rotating turret Vickers hardness tester (model YZHV−1000Z), with an applied load of 10 N and a dwell time of 10 s. The wear resistance of the coatings was evaluated using a linear reciprocating Bruker (CETR) UMT−2 tribometer, which provided friction coefficient curves and three-dimensional wear morphologies. The friction pair consisted of a 6 mm-diameter alumina ball with a test time of 30 min and an applied load of 15 N. Additionally, the friction velocities and strokes were set as 10 mm/s and 3 mm, respectively. In addition, the adhesion strength between the coating and copper alloy substrate was assessed using the micro-scratch method with an Anton Paar NHT+MCT instrument, in the load range of 0−30 N The scratch velocity and length were set as 5 mm/min and 5 mm, respectively.

2.4 First-principles calculation

The first-principles calculations conducted in this study employed the Vienna Ab initio Simulation Package (VASP) program. The Projector Augmented Wave (PAW) method [14] was used to describe interactions between the real ions and valence electrons, and the Perdew-Burke-Ernzerhof (PBE) function, based on the generalized gradient approximation (GGA), was employed to handle the exchange-correlation potential. In the computational process, a plane-wave cutoff energy of 450 eV was set to ensure good convergence, with convergence energy and force criteria of 1×10^{-6} eV and 1×10^{-3} eV/Å, respectively. The Monkhorst−Pack method [15] was used for Brillouin zone sampling in reciprocal space, employing a 10×10×7 *k*-point grid. Additionally, considering the magnetic properties of the systems, the calculations were performed with spin polarization taken into account.

3 Results and discussion

3.1 Electrodeposition process optimization of Ni−Co−C alloy coatings

3.1.1 Carbon source

The deposition behavior of carbon significantly differs from the electroplating of traditional metals. Ionizing carbon into elemental ions in a deposition solution using a simple salt-like material and achieving complete deposition on the cathode surface posed significant challenges. After conducting a comparative analysis of the existing deposition methods for carbon atoms (S2 in SM), we used oxalic acid, ammonium oxalate, sodium oxalate, and urea as the carbon-containing inorganic chemical reagents and carbon sources. Our aim was to deposit a carbon film on a cathode copper alloy. The composition of the deposited solution and the parameters of the electroplating process are provided in Table S1 of SM.

The experimental results indicated that when oxalic acid and urea were used separately as carbon sources, based on the macroscopic morphology of the deposited surface of the copper plate, the cathode surface consistently remained bright brown, and no new material was produced. This observation suggests that C element could not be deposited onto the cathode. When sodium oxalate was used as the carbon source, a small number of extremely uneven dark gray spots appeared on the surface of the cathode copper plate, which was possibly related to the poor conductivity of the deposited solution. In contrast, when ammonium oxalate was employed as the carbon source, a uniform, dark gray film formed on the copper plate, resembling the appearance of dark nickel.

The surface of the film was characterized by SEM and EDS, as illustrated in Fig.1. The results revealed a complex surface structure with numerous folds and pits, similar to the morphology of amorphous carbon films obtained by CHE et al through electroplating [16]. Additionally, as shown in Fig. 1(b), the primary component of the film was carbon, distributed uniformly. Consequently, using ammonium oxalate as the carbon source successfully deposited C element on the cathode, laying the foundation for further research.

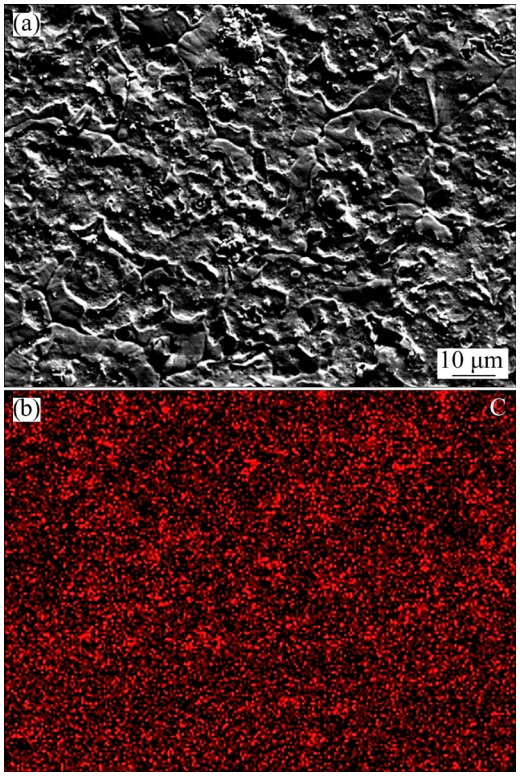

Fig. 1 SEM image (a) and EDS result (b) of cathode surface films

3.1.2 Effective coordination agents

When using ammonium oxalate as the carbon source, the presence of an effective coordination agent can prevent the insoluble precipitation of oxalate ions and metal ions in the deposited solution. This is crucial for achieving the co-deposition of Ni, Co and C elements. We selected several commonly used coordination agents for electrodepositing nickel or cobalt-based alloy coatings, including sodium formate, sodium acetate, sodium citrate, ammonium citrate, and urea [17−19], as the screening basis. Additionally, studies have shown that under certain conditions, the use of double coordination agents can yield better complexing effects compared to single coordination agents [20]. We also employed partial combinations of the aforementioned coordination agents. We aimed to select an optimal coordination agent component by comparing and analyzing the state, stability, and coating hardness of the deposited solution. The experimental systematics and process parameters for electrodeposition were provided in Table S2 of SM.

The experiments were organized into six groups, as outlined in Table S3 of SM. The addition of sodium formate, sodium acetate, and urea as coordination agents resulted in a poor complexation effect, evident from the formation of insoluble precipitates and turbidity in the deposited solution. When sodium citrate was used as the coordination agent, the pre-deposition solution appeared clear; however, post-deposition, turbidity was observed, indicating instability of the deposited solution resulting in lower coating hardness. In contrast, when ammonium citrate was employed as the coordinating agent, Ni^{2+} and Co^{2+} were effectively complexed, resulting in a clear deposition solution without precipitation and exhibition good uniformity. Additionally, the prepared coating demonstrated superior surface quality and performance.

When ammonium citrate dissolved in an aqueous solution, it underwent decomposition, yielding three ammonium ions and anions, as shown in Eq. (1). Furthermore, as indicated in the literature [18], when dissolved in water, ammonium citrate will chemically react with the metal cations (hereafter referred to as M^{2+}) in the deposition solution, as depicted in Eqs. (2) and (3), thereby achieving effective chelation. Additionally, the ammonium ions derived from the decomposition of ammonium citrate could form a series of complexes with metal ions, particularly $M(NH_3)_3^{2+}$, which could enhance the chemical activity of metal ions and facilitate their cathodic deposition [21].

Therefore, ammonium citrate effectively chelated metal ions and enhanced cathodic reduction activity, making it a valuable coordinating agent for the electrodeposition of Ni−Co−C alloy coatings. Moreover, when sodium citrate was combined with ammonium citrate, the deposition solution remained clear and stable. However, the coating hardness slightly decreased compared with using ammonium citrate alone. Consequently, after a comprehensive comparison, ammonium citrate was selected as the coordinating agent in the Ni−Co−C coating preparation systems.

$$C_6H_5O_7(NH_4)_3 \rightarrow C_6H_5O_7^{3-} + 3NH_4^+ \quad (1)$$

$$C_6H_5O_7^{3-} + M^{2+} \rightarrow MC_6H_5O_7^- \quad (2)$$

$$MC_6H_5O_7^- + C_6H_5O_7^{3-} \rightarrow M(C_6H_5O_7)_2^{4-} \quad (3)$$

Expanding upon the experimental parameters detailed in Table S2 of SM, single-factor experiments were conducted. These experiments

involved varying the carbon source (ammonium oxalate) content in the range of 10−50 g/L, adjusting the current density (3−8 A/dm²), and varying the temperature (30−70 °C) and $CoSO_4$ content (1−5 g/L). The optimal preparation process was determined through a comprehensive evaluation and comparison of the coating composition, surface quality, microscopic morphology, and hardness. This experimental procedure included adjusting the pH of the deposition solution using dilute sulfuric acid or NaOH solution to stabilize the solution within a specific range.

3.1.3 Effects of electrodeposition process parameters on coating morphology, composition and properties

(1) Ammonium oxalate content

The carbon content in the deposition solution was closely related to the carbon content in the final coatings and significantly influenced the surface morphology, quality, and performance of the coatings. The mechanism responsible for the deposition of C atoms during the electro- deposition of oxalates was not well understood at the time. Presumably, ammonium oxalate ionizes in the deposited solution. Subsequently, the oxalate ions migrated to the cathode under the influence of the electric field and underwent electron reduction, ultimately completing the deposition of carbon, as shown in Eqs. (4) and (5). Additionally, ionized ammonium ions could form complexes with metal ions, enhancing their cathodic activity and facilitating the reduction of metal cations [21]:

$$(NH_4)_2C_2O_4 \rightarrow C_2O_4^{2-} + 2NH_4^+ \quad (4)$$

$$C_2O_4^{2-} + 8H^+ + 6e \rightarrow 2C + 4H_2O \quad (5)$$

Figure S2 of SM presents the surface morphology of the coatings under various concentrations of ammonium oxalate in the deposition solution. The coated surfaces displayed inhomogeneous characteristics with varying sizes of granular features. As the ammonium oxalate concentration increased, the coating surface transitioned from a mixed granular structure to a cellular structure. This transition was characterized by the tendency for grain aggregation, leading to the formation of numerous clusters. Further increase in ammonium oxalate content resulted in the appearance of cracks on the coating surface, including intragranular cracks (red circles) and transgranular cracks (blue circles). The subsequent analysis of the composition and hardness of the coatings at different ammonium oxalate concentrations was presented in Fig. S3 of SM. We observed that the carbon content in the coating was positively correlated with the ammonium oxalate content in the deposited solution. Moreover, as the carbon content in the coating increased, the Ni and Co contents approached a more balanced ratio of 1:1.

The electrodeposition of Ni−Co alloy involved an anomalous co-deposition process, wherein Co^{2+} ions, possessing a higher electrode potential, exhibited a greater tendency for reduction and deposition on the cathode surface compared to Ni^{2+} ions with a lower electrode potential [22]. DAHMS and CROLL [23] proposed that the anomalous co-deposition behavior was primarily attributed to the formation of $Co(OH)_2$, which impeded the reduction of Ni^{2+} ions and adsorbed onto the cathode. Interestingly, a competitive trend between the deposition of C and Ni was observed in this study. Furthermore, an increase in C content intensified the aforementioned anomalous co-deposition phenomenon, thereby favoring Co deposition.

In addition, there was a well-established correlation between the hardness of the coatings and their C content. Specifically, as the C content increased, the hardness rose and stabilized at an elevated level. Notably, the higher C content resulted in tighter binding between the coated grains, positively impacting overall performance. Consequently, the hardness remained high despite the appearance of cracks in the coatings at higher C content. Clearly, the hardness of the coatings was influenced by their composition, mass, and structural properties. At a concentration of 30 g/L of ammonium oxalate, the coating exhibited the highest C content (2.1 wt.%) and simultaneously achieved the maximum hardness (HV 699.1). This represented an approximately 32% increase in hardness compared with the binary alloy coating with a similar nickel–cobalt ratio (HV 530).

(2) Current density

The current density was also considered a crucial parameter affecting the quality and performance of the coatings during electro-deposition. Figure S4 of SM illustrates the surface microstructure of the Ni−Co−C alloy coatings at various current densities ranging from 3 to 8 A/dm².

The effect of the current density on the coating morphology was relatively minor, with the coatings consistently maintaining an irregular, granular appearance. However, at higher current densities (≥7 A/dm²), the coating's surface exhibited deep cracks that continuously propagated between the grains. This was mainly attributed to the increased mobility of ions in the deposition solution at elevated current densities. Hence, a higher current density increased the number of cations reaching the cathode surface per unit time, facilitating the reduction process and accelerating the coating growth rate [24]. During this competitive growth process, the continued enlargement of the coated grains resulted in a gradual increase in internal stress. Once, this internal stress exceeded a critical threshold, it induced cracking in the coating, significantly affecting the quality and performance of coating.

Similarly, the effect of current density on the coating composition and hardness was investigated, as shown in Fig. S5 of SM. The current density had a more pronounced effect on the coating composition than the ammonium oxalate content. Specifically, the Ni content in the coatings consistently increased with higher current density, while the Co content steadily decreased. This was attributed to the increased cathodic polarizability during the electrodeposition process at higher current densities [25], which favored the deposition of Ni^{2+} ions at lower electrode potentials while suppressing the deposition of Co^{2+} ions.

However, the variation in C content in the coatings showed no distinct trends with changes in current density, while the hardness first increased and then decreased. At excessively high current densities, the coated surface tended to char, darken, undergo severe hydrogen evolution, and develop pores, resulting in a porous and less dense structure with reduced hardness. Notably, at a current density of 4 A/dm², the coating exhibited the highest hardness, presenting a uniform and smooth surface without visible defects.

(3) Electrolyte temperature

The temperature of the solution used during electroplating directly affected the growth and crystalline properties of the coatings, which in turn affected their surface quality and overall performance [26]. As the temperature increased, the deposition potential of the solution became more positive, effectively reducing cathodic polarization and promoting an increase in the cathodic current density and deposition rate. However, excessive temperature might reduce the stability of the deposited solution [24].

The microstructure, composition, and temperature-dependent characteristics of the coatings at different deposition temperatures were illustrated in Figs. S6 and S7 of SM. The experimental results revealed severe cracking defects on the coating surface at 30 °C. These cracks were deep and wide, penetrating the entire surface, and resulting in an extremely low coating hardness of HV 464.7, even lower than that of the binary Ni−Co alloy. This analysis suggested that at low temperatures, the decreased activity of the constituents in the deposited solution and the slower mass transfer rate between particles result in slower coating growth and reduced inter-grain binding strength. The accumulation of internal stress during electro-deposition initiated and rapidly propagated microcracks, ultimately forming wide and deep cracks that significantly impacted the coating performance. As the temperature increased, the coating growth rate accelerated, the crack defects gradually diminished, the coating surface became smoother, and the grain size became more uniform, consistent with the findings of RADADI et al [27]. Additionally, the increase in temperature also promoted an enhancement in the coating hardness.

Furthermore, the influence of temperature on the coating composition was greater than the current density. As the temperature increased, both the Co and C contents in the coating initially increased and then decreased, following a consistent pattern with hardness changes. This indicated that excessively high or low temperatures were unfavorable for the deposition of Co and C. Notably, at a deposition solution temperature of 50 °C, the coating exhibited the highest C content, with a bright surface that contained no cracks or pores, and achieved peak hardness.

(4) Principal salt concentration

The optimal preparation process for the Ni−Co−C alloy coatings was determined as follows: ammonium oxalate concentration of 30 g/L, current density of 4 A/dm², and a deposition temperature of 50 °C. Under these conditions, the resulting coating exhibited a dense crystallinity, and a surface devoid of noticeable defects such as cracks or pores, thus

achieving maximum hardness.

The concentration of principal salt in the deposited solution also significantly affected the composition and properties of the coatings. Previous research has indicated the significant impact of Co content on the organizational structure and hardness of binary Ni−Co alloys [28]. Specifically, the coating hardness steadily increased as the Co content increased; however, with high Co content, the coating underwent a transition from FCC to HCP, resulting in a subsequent decrease in hardness. Therefore, the effect of $CoSO_4$ concentration in the deposited solution under optimal conditions on the coating quality, composition, and properties was investigated, as depicted in Figs. S8 and S9 of SM. The experimental results revealed that increasing the $CoSO_4$ concentration led to a continuous increase in the Co content in the coatings and a decrease in the Ni content, while the C content remained relatively stable. Consequently, the increase in Co^{2+} ions in the deposited solution significantly inhibited the deposition of Ni^{2+} ions, exacerbating anomalous co-deposition behavior.

In addition, the $CoSO_4$ concentration strongly affected the coating morphology. At lower $CoSO_4$ concentrations, the coated surface exhibited low-density clustered grains. As the $CoSO_4$ concentration increased, the clusters gradually dispersed into uneven and denser grains, accompanied by a gradual increase in coating hardness. The enhanced hardness at this stage is attributed to the continuous elevation of Co content.

3.2 Microstructure and performance of Ni−Co−C coatings

3.2.1 SEM, XRD and XPS characterization

Figure 2 depicts the surface morphology of the Ni−Co−C alloy coatings characterized by SEM and analyzed by EDS surface scans. Optimized coated surfaces exhibited distinct granular features with dense fine-grained crystalline structures, where large grains combined to form numerous clusters of densely distributed nanoscale particles on their surfaces. Additionally, the EDS elemental distribution maps revealed that the coating was composed of three elements, namely Ni, Co, and C, which were uniformly distributed.

The crystal structure of the coatings was characterized by X-ray diffraction (XRD), as shown in Fig. 3. Comparative analysis was performed using the XRD spectra of pure Ni with a face-centered cubic (FCC) structure and a Ni−Co binary alloy coating with a composition similar to that of the Ni−Co−C alloy coating. Both the Ni−Co and Ni−Co−C alloy coatings exhibited XRD peaks similar to those of pure Ni, indicating a single-phase FCC structure without any additional diffraction peaks. Therefore, the doping of C did not alter the original crystal structure of the alloy or induce the formation of new phases. Furthermore, changes in the intensity of various diffraction peaks indicated that the addition of C changed the preferred orientation of the coatings, specifically manifesting as a reduction in the (200) crystal plane peak and an enhancement in the (220) crystal plane peak.

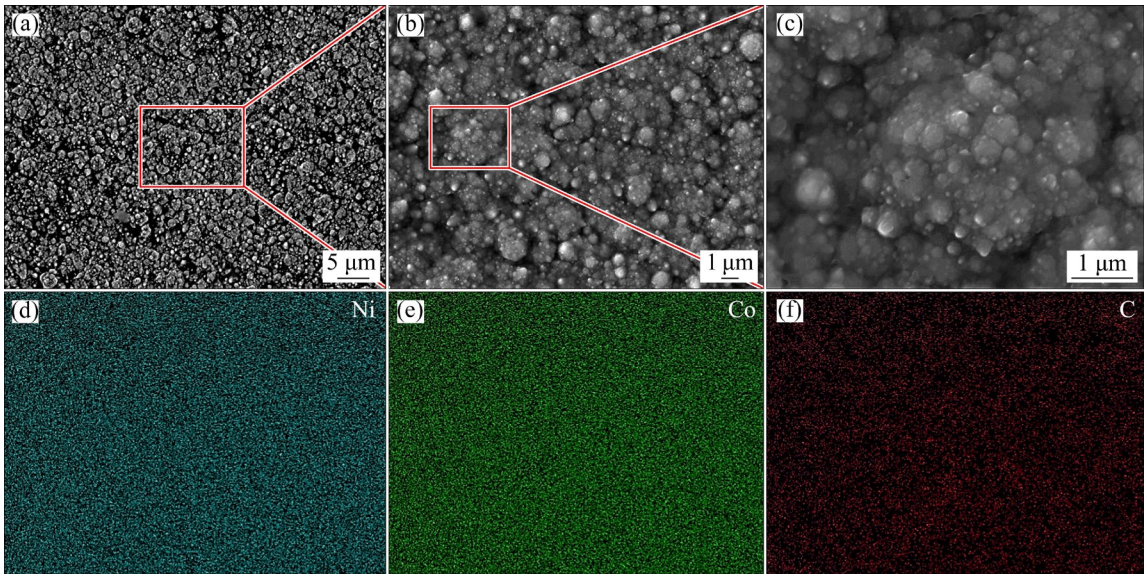

Fig. 2 SEM images (a−c) and corresponding EDS elemental distribution maps (d−f) of Ni−Co−C alloy coating

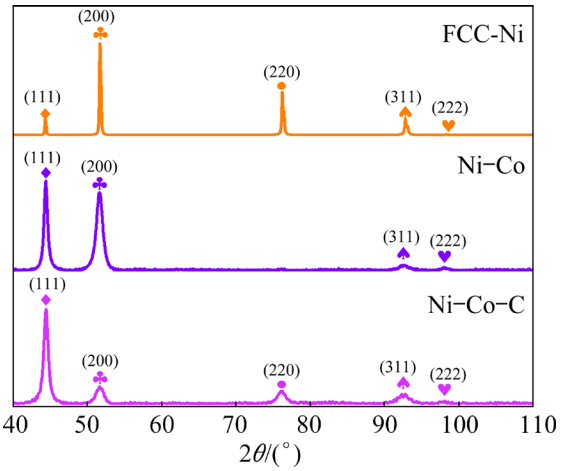

Fig. 3 XRD patterns of FCC-Ni, Ni−Co and Ni−Co−C

On this basis, we calculated the lattice constants of the coatings using the (111) crystal plane diffraction parameters and Eqs. (6) and (7) [29]:

$$d=\frac{\lambda}{2\sin\theta} \tag{6}$$

$$a=d\cdot\sqrt{h^2+k^2+l^2} \tag{7}$$

where d is the crystal plane spacing; λ represents the wavelength of the diffraction wave, which is 0.15406 nm; θ is the diffraction angle; a is the lattice constant; h, k and l are the crystal plane indices. Meanwhile, according to the Scherrer formula [30] (Eq. (8)), we calculated the change in coating grain size (D) after the doping of C element.

$$D=\frac{K\lambda}{\beta\cos\theta} \tag{8}$$

where K is a constant, taken as 0.9 [31], and β is the full width at half maximum of the diffraction peak. The detailed calculations were provided in Table 1. It was observed that the doping of C element expanded the lattice of Ni−Co coating and increased distortion, thus resulting in an increase in its lattice constant. In addition, the grain size of Ni−Co coating was 41.16 nm, which was close to relevant research results [32,33], while the grain size of Ni−Co−C coating was 30.59 nm, indicating that the doping of C element effectively reduced the grain size of Ni−Co alloy coatings. According to the Hall−Petch relationship [34], the refinement of grains is beneficial for improving the overall performance of the coatings.

Table 1 Lattice constants and grain sizes of Ni−Co and Ni−Co−C coating

Coating	Lattice constant/Å	Grain size/nm
Ni−Co	3.528	41.16
Ni−Co−C	3.531	30.59

To further elucidate the bonding and oxidation states of each element in the coatings, X-ray photoelectron spectroscopy (XPS) characterization was conducted, as depicted in Fig. 4. Four elements, namely, Ni, Co, C and O, were primarily detected on the surface of the coatings. The presence of O was possibly due to localized oxidation or by-products introduced during electrodeposition, such as metal hydroxides. Based on this result, peak fitting was performed on the characteristic spectra of the measured elements. Figures 4(b)−(d) represent the fine spectra corresponding to the C, Ni, and Co elements. It is observed that the C 1s fitting peaks primarily consisted of two peaks at 284.8 (C^0 [35]) and 287.9 eV (C═O [36]). The C^0 peak, with a higher intensity, represented the dominant form of carbon in the coatings. By contrast, the C═O peak was weaker, most likely due to partial oxidation on the coated surface. Therefore, in conjunction with XRD analysis, we inferred that C was primarily present in atomic form and solidly dissolved in the coatings. This enhancement in the coating hardness was mainly attributed to the solid-solution strengthening and grain refining resulting from the C atoms.

In addition, Ni exhibited four characteristic peaks. Among them, Ni $2p_{1/2}$ and Ni $2p_{3/2}$ were observed at 852.6 and 869.8 eV, respectively. The peaks at 852.6 and 869.8 eV were attributed to Ni^0 [37,38], while the other two peaks corresponded to Ni^{2+} [38,39]. Specifically, other than in the form of metallic Ni, Ni^0 was also present in the form of NiCo in the coatings, while Ni^{2+} ions mainly existed in the form of $Ni(OH)_2$ [39]. Similarly, Co exhibited mainly three characteristic peaks. Among them, Co $2p_{1/2}$ and Co $2p_{3/2}$ were observed at 778.1 and 793.4 eV. The peaks at 778.0 and 793.4 eV were attributed to Co^0 [37,40], while the peak at 781.0 was assigned to Co^{2+} [41]. Analogous to Ni, Co^0, other than existing as metallic Co, was also present in the form of CoNi in the coatings, while Co^{2+} ion was mainly present in the form of $Co(OH)_2$ [40].

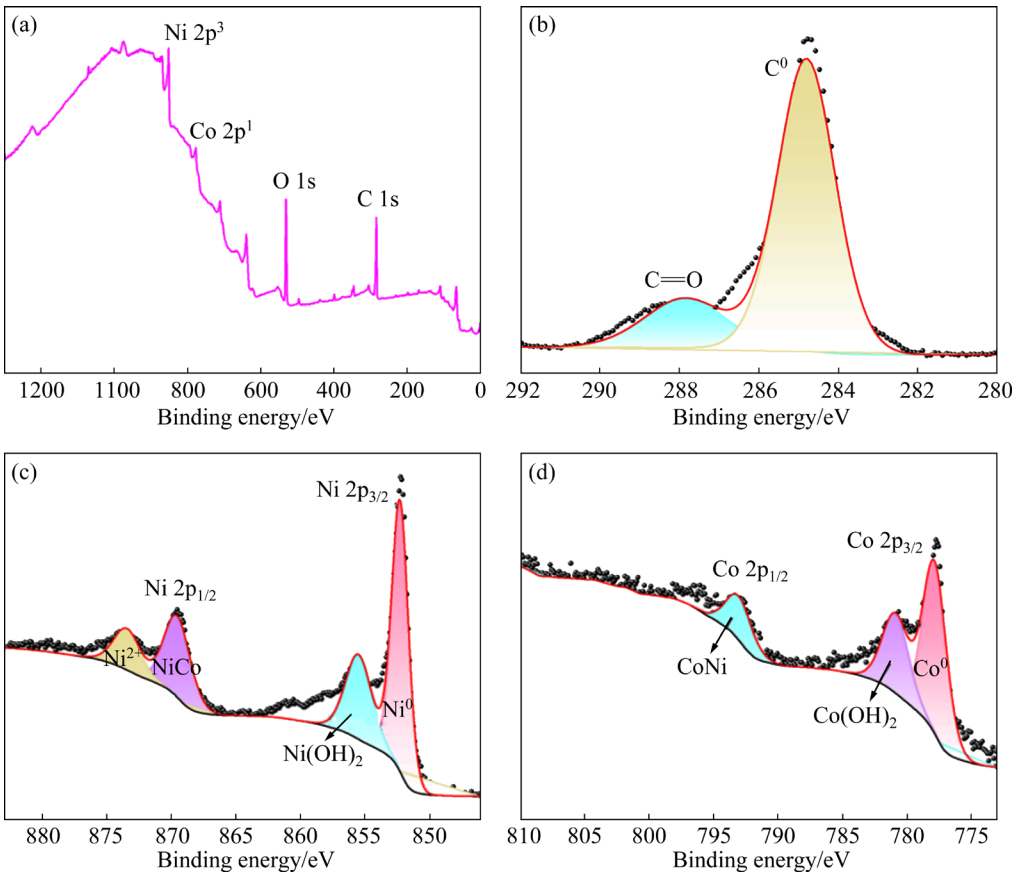

Fig. 4 XPS spectra of Ni−Co−C coating: (a) Survey; (b) C 1s; (c) Ni 2p; (d) Co 2p

Notably, during electrodeposition, two side reactions occurred at the cathode, namely, the hydrogen evolution reaction and the electrolysis of water, as shown in Eqs. (9) and (10). Ni^{2+} ions and Co^{2+} ions reacted with OH^- ions migrating to the cathode to form metal hydroxides (Eq. (11)), with Co^{2+} ions preferentially reacting. However, the presence of Co (OH) $_2$ hindered Ni deposition by reducing the active sites on the cathode, leading to the anomalous co-deposition characteristics of the Ni−Co alloy. Additionally, metal hydroxides that were not promptly deposited were present in the coatings as by-products. Figure 5 schematically illustrates these reactions [22].

$$2H^+ + 2e \rightarrow H_2 \quad (9)$$

$$2H_2O + 2e \rightarrow H_2 + 2OH^- \quad (10)$$

$$M^{2+} + 2OH^- \rightarrow M(OH)_2 \quad (11)$$

3.2.2 Wear resistance and adhesion strength

Excellent wear resistance served as a fundamental requirement for coatings used in molds. In this study, Ni−Co−C alloy coatings were prepared using the optimal electrodeposition process, with

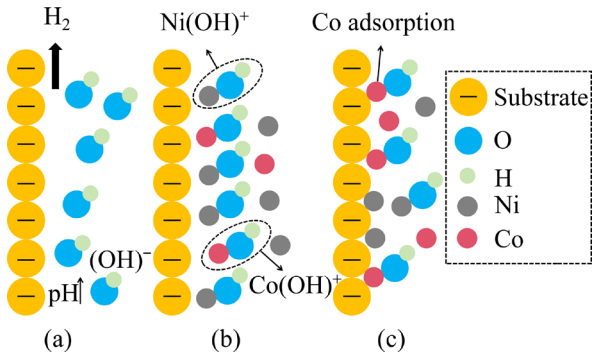

Fig. 5 Schematic diagrams showing abnormal co-deposition of Ni−Co alloy: (a) Hydrogen evolution reaction; (b, c) Metal deposition

composition of Ni 52.1 wt.%, Co 45.8 wt.%, and C 2.1 wt.%, as well as Ni to Co mass ratio of 1.14. Additionally, a binary alloy with a similar Ni to Co mass ratio was prepared for comparison, using the following deposition process: 100 g/L of $NiSO_4 \cdot 6H_2O$, 10 g/L of $CoSO_4 \cdot 7H_2O$, 40 g/L of $NiCl_2 \cdot 6H_2O$, 30 g/L of boric acid, 0.2 g/L of sodium dodecyl sulfate, 0.4 g/L of saccharin, a current density of 4 A/dm^2, and a deposition temperature of 40 °C. The resulting binary Ni−Co alloy

composition was Ni 51.8 wt.% and Co 48.2 wt.%, with a nickel–cobalt mass fraction ratio of 1.07, which closely matched that of the ternary alloy coating. This similarity made it highly valuable for comparative research.

The coefficient of friction (COF) served as a crucial parameter for assessing the wear resistance of materials and, is typically associated with their hardness and surface characteristics [42]. Figure 6(a) showed the variations in the COF over time for Ni−Co and Ni−Co−C alloy coatings. Initially, the COF for the Ni−Co coating rapidly increased, stabilized after 400 s, and demonstrated a slow increasing trend. This was primarily attributed to the high surface roughness of the coatings, with numerous protruding particles on the surface. During the initial stages of frictional wear, the coating surface sustained damage, resulting in a rapid increase in the COF due to the generation of a large number of frayed fragments over a short period of time. With prolonged time, the protruding particles gradually wore down. At this juncture, contact between the frictional pair and the coated surface transitioned from multiple point contacts to surface contacts, leading to a gradual stabilization of the COF as frictional wear entered a dynamic equilibrium phase.

By contrast, for the Ni−Co−C alloy coatings, the COF increased more gradually and more uniformly, consistently staying below 0.15. Importantly, the average COF for the Ni−Co−C alloy coatings was 0.13, which was 70.5% lower than that of the binary alloy, demonstrating a significant improvement in wear resistance due to the addition of C element. Using the average COF as a reference, the wear resistance of the ternary Ni−Co−C alloy coatings was 3.4 times higher than that of the binary alloys. In addition, Figs. 6(b−e) presented the wear volume and wear morphology of the Ni−Co and Ni−Co−C alloy coatings. We observed that the wear mass and wear volume of the Ni−Co−C alloy coatings are 0.04 mg and 4.57×10^{-4} mm^3, respectively, representing 42.8% and 45.4% reduction compared to the binary alloys,

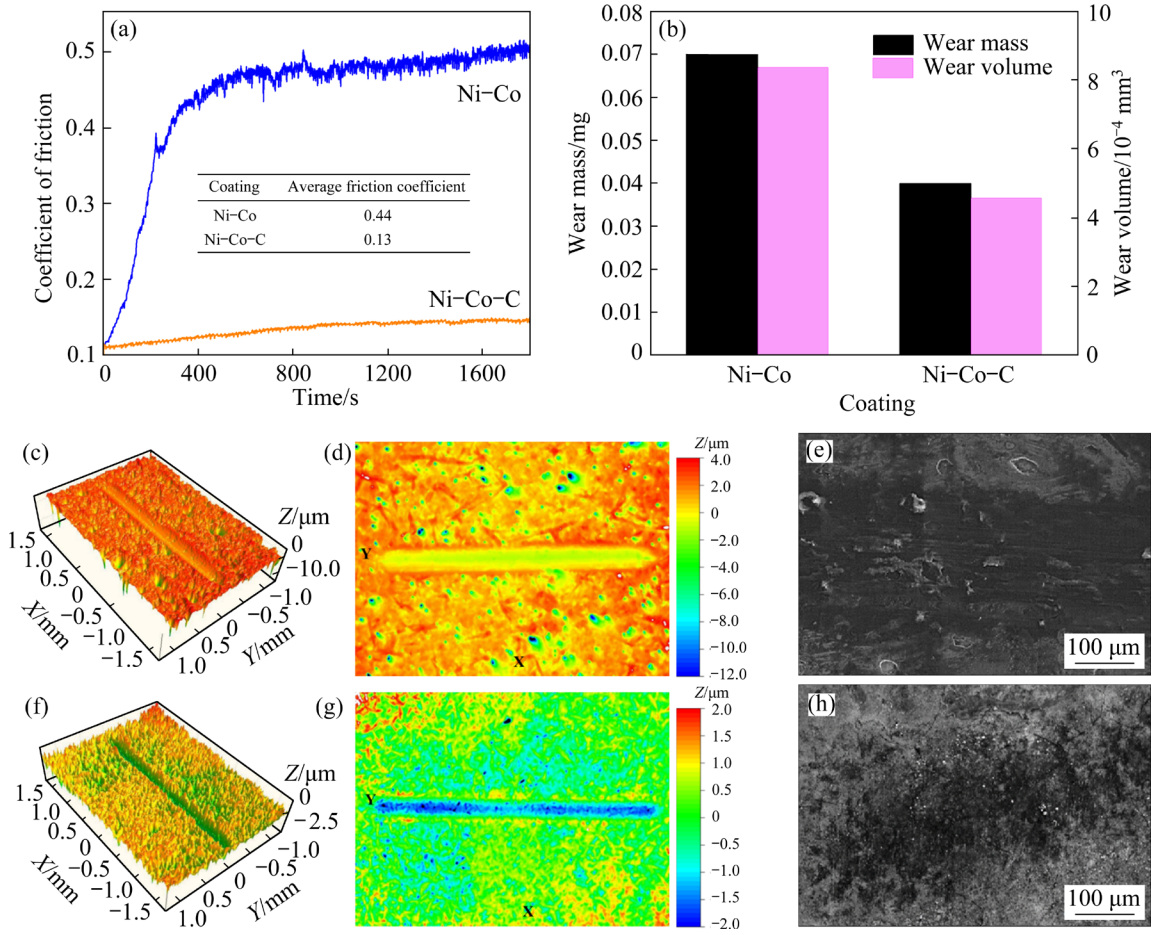

Fig. 6 Wear properties of Ni−Co and Ni−Co−C alloy coatings: (a) Coefficient of friction; (b) Wear mass and wear volume; (c−e) Wear morphology of Ni−Co coating; (f−h) Wear morphology of Ni−Co−C coating

indicating outstanding wear resistance. Notably, for this study, doping with C element significantly improved the microhardness of the Ni−Co alloy coatings. Additionally, the wear resistance of Ni−Co−C alloy coating was proportional to the microhardness according to the Archard wear relation [43], as shown in Eq. (12). Moreover, the wear volume was inversely proportional to the hardness when the friction and wear experimental conditions were consistent. Hence, doping with C element increased the hardness of the Ni−Co alloy coatings, further improving their wear resistance, as clearly obtained from the detection results of the COF, the wear volume and the wear quality:

$$\frac{V}{S}=\frac{K\cdot F_{\mathrm{N}}}{H} \tag{12}$$

where V is the wear volume, S is the stroke distance of the frictional pair, K represents the COF, and F_{N} and H denote the load and microhardness of the coatings, respectively.

Moreover, Figs. 6(c−e) and 6(f−h) illustrated the wear morphologies of the Ni−Co and Ni−Co−C alloy coatings, respectively. The significantly reduced wear depth and width of the Ni−Co−C coatings compared with the binary coatings confirmed that the addition of C element effectively enhanced the wear resistance of the coatings. The wear marks on the surface of the Ni−Co coatings were very pronounced, with an uneven surface and residual wear debris, indicating a mixing mechanism of abrasive wear and adhesive wear. This was mainly due to high contact stress between the substrates and the frictional pair during the experiment and the low hardness of the Ni−Co coatings, leading to significant plastic deformation during friction and partial detachment with shear stress. In comparison, the Ni−Co−C alloy coatings, due to their higher hardness, could more effectively resist the indentation of the frictional pairs into the coatings and the shear motion during the wear process. We observed that the protruding particles on the coated surface were not completely worn down, with only slight wear marks and no extensive peeling.

The excellent bonding performance between the coatings and the substrates served as a prerequisite for its smooth and efficient application. In this study, the micro-scratch methods were used to assess the bonding strength between the coatings and the substrates. Unlike the wear resistance tests, we controlled the deposition time to maintain the thickness of both the Ni−Co binary and Ni−Co−C alloy coatings at around 5 μm to eliminate the influence of coating thickness on the experimental results and ensure that the indenter could smoothly penetrate the coatings. Each sample underwent three repeated scratch experiments at different positions, and the critical load was comprehensively determined by changes in tangential frictional force, indenter penetration depth, and scratch morphology.

Figure 7 presented the experimental micro-scratch results for the Ni−Co binary and Ni−Co−C alloy coatings. In the early stages of the experiments, both the coatings exhibited a relatively uniform increase in tangential frictional force and penetration depth. As the indenter moved forward

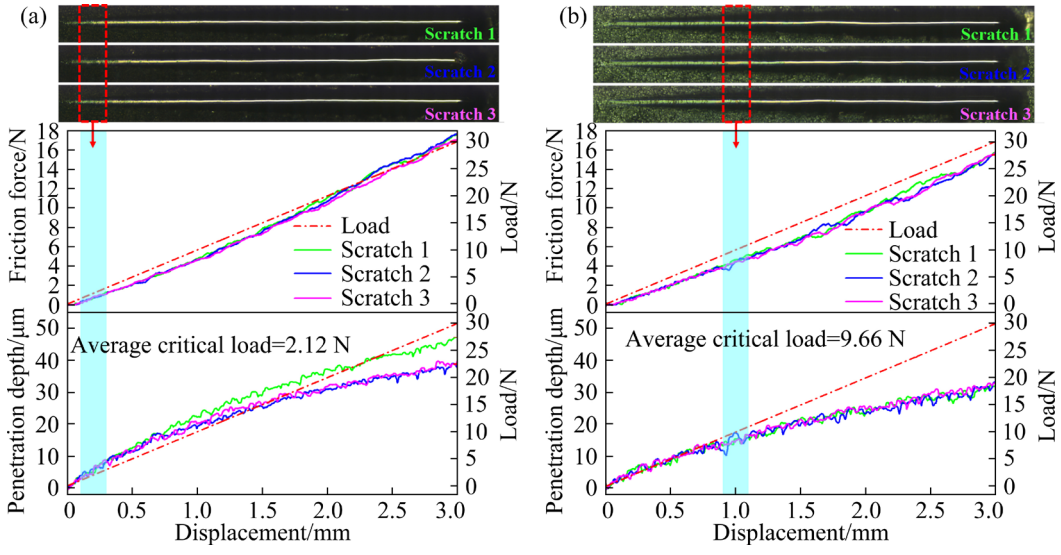

Fig. 7 Adhesion strength of Ni−Co coating (a) and Ni−Co−C coating (b)

with increasing load, the growth of frictional force and penetration depth became erratic when the load reached a certain value, and this phenomenon became more pronounced in the ternary coatings. Furthermore, it was clear that when approaching the critical load, the coatings noticeably delaminated from the substrates, demonstrating the bonding strength between the coating and the substrates measured by this critical load. The critical load for the indenter penetrating the Ni−Co−C coating was 9.66 N, which was 4.6 times that of the binary coatings. The above experimental results demonstrated that the doping of C element could effectively enhance the hardness and wear resistance of the Ni−Co alloys while simultaneously strengthening the interfacial bonding performance between the coatings and the copper substrates.

3.3 Performance enhancement mechanism of Ni−Co−C alloy coatings

To elucidate the reinforcing mechanism introduced by C atoms at the microscopic atomic bonding and electron distribution level, we employed first-principles calculation methods to establish a C-doped Ni−Co alloy model. A detailed analysis of the local electronic properties is presented in Fig. 8, and details regarding model construction can be found in S5 of SM. Prior to the calculations, structural relaxations were performed on the bulk models of pure Ni and pure Co. The lattice constants obtained for Ni (FCC) were $a=b=c=3.52$ Å, and for Co (HCP), $a=b=2.51$ Å, $c=4.07$ Å. These values were closely aligned with previous studies [44−46], validating the reliability of our computational approaches.

Figure 8(a) presented the total density of states (TDOS) and local partial density of states (PDOS) for the system. It was evident that the TDOS between −8 and −6 eV was mainly due to the C 2p orbitals, and contributions from the Ni and Co 3d orbitals were predominant beyond −6 eV. In addition, a continuous distribution of states at the Fermi level with a 0 bandgap indicated the typical metallic properties [47]. Notably, the contribution

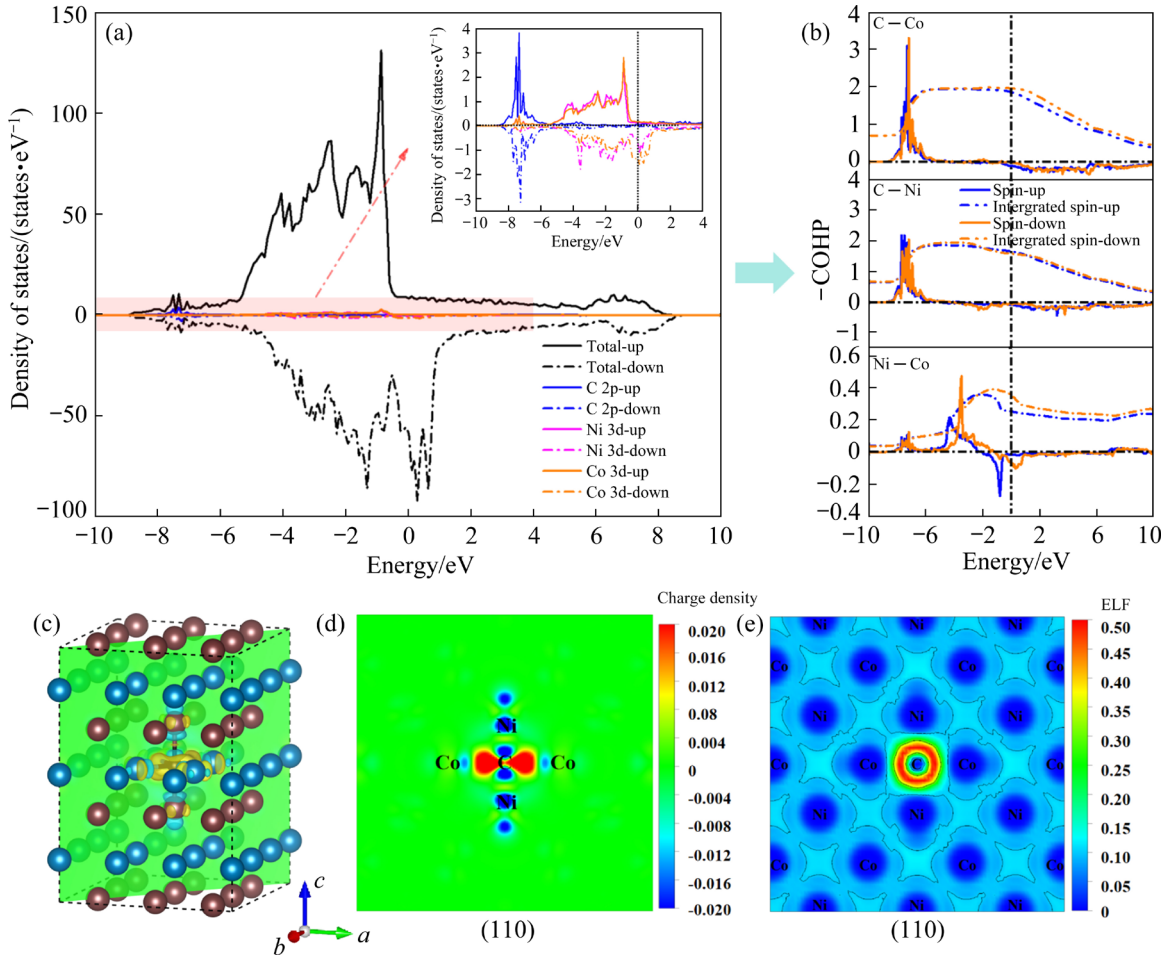

Fig. 8 Electronic properties of Ni−Co−C alloy coating: (a) DOS; (b) COHP; (c, d) 3D differential charge density and projection, respectively; (e) ELF

of spin-up electrons to the TDOS was more significant. Notable hybridization was observed between the C 2p orbitals and metal 3d orbitals across the entire electron range, suggesting significant overlap and strong interactions between the outer electrons of the corresponding nuclei.

To elucidate the origin of this strong interaction, we calculated the crystal orbital Hamilton population (COHP) and corresponding integrated curves for the relevant atomic pairs to quantify the contributions of bonding and antibonding orbitals from a molecular orbital perspective. The results indicated substantial contributions from both spin-up and spin-down electron pairs in the bonding orbitals between the C−Ni and C−Co atomic pairs. In numerical terms, the bonding strengths were ranked as follows: C−Co>C−Ni>Ni−Co. This suggested that the addition of C atoms significantly enhanced the local atomic bonding capability in the NiCo bulk, which could potentially contribute to the improved coating hardness and wear resistance.

To visually illustrate the charge transfer and distribution characteristics before and after C atom doping, we computed the differential charge density and electron localization function (ELF) of the system. Figures 8(c) and (d) depicted the 3D differential charge density map and its projection on the (110) crystal plane, where in the 3D differential charge density map, the yellow and cyan regions represented charge accumulation and loss, respectively [48]. In addition, for ELF, a critical value of 1 or 0 indicated whether the charge was in a localized or delocalized state, corresponding to either covalent interactions or ionic bonds [49]. The addition of C atoms led to the aggregation of local charges, while the charge density around Ni and Co atoms decreased, suggesting partial charge transfer from metal atoms toward the vicinity of the C atoms. Furthermore, ELF calculations revealed that the electron distribution between Ni−Co and Ni−Ni atoms exhibited a delocalized state, which was consistent with the results of the DOS analysis. With the introduction of C atoms, the electron distribution in the corresponding region became more localized, concurrently promoting transition from weak ionic bonds to strong covalent bonds. Therefore, C atoms primarily enhanced bonding between relevant atoms in the NiCo bulk by modulating the local charge density and electron distribution, ultimately enhancing the overall mechanical performance of the coatings.

4 Conclusions

(1) The utilization of an ammonium oxalate–citric acid system ensured the successful deposition of carbon atoms while maintaining high stability of the deposited solution. After conducting a comprehensive assessment of coating composition, morphology, quality, and performance through single-factor experiments, the optimal preparation parameters were determined as follows: ammonium oxalate concentration of 30 g/L, current density of 4 A/dm², and a deposition solution temperature of 50 °C.

(2) The optimized coatings exhibited dense crystallization, presenting a distinct granular structure. The surfaces of large-sized particles exhibited a concentrated distribution of nanoscale particle clusters. Furthermore, C atoms were mainly present within the coatings in a solid solution, preserving the original FCC structure without alteration.

(3) The adding of C element resulted in a significant enhancement in the coating's performance. Specifically, the coating's hardness increased by 32%, and its adhesion strength was 4.2 times higher than that of the binary coating. Moreover, notable reductions in the coating's coefficient of friction, wear volume, and wear mass were observed.

(4) The introduction of C atoms optimized the local charge density and electron distribution within the alloy, leading to a transformation from weak ionic bonds to strong covalent interactions in specific regions. This enhanced the bonding capacity among corresponding atoms in the NiCo bulk, resulting in an improvement in the alloy's overall performance.

CRediT authorship contribution statement

Yi-zhe DU: Conceptualization, Methodology, Writing – Original draft; **Zhen-yao CHEN** and **Hua-mei DUAN:** Data curation; **Mu-jun LONG:** Investigation, Resources; **Deng-fu CHEN:** Investigation, Supervision, Funding acquisition.

Declaration of competing interest

The authors declare that they have no known competing financial interests or personal relationships that could have appeared to influence the work reported in this paper.

Acknowledgments

This work was supported by the National Natural Science Foundation of China (Nos. 52274320, 52074053).

Supplementary Materials

Supplementary Materials in this paper can be found at: http://tnmsc.csu.edu.cn/download/16-p2683-2024-0029-Supplementary_Materials.pdf.

References

[1] ZHANG Cheng-zhi, ZHANG Xing, WU Jing-feng, ZHU Ling-jun, WANG Shu-rong. Hydrodeoxygenation of lignin-derived phenolics to cycloalkanes over Ni−Co alloy coupled with oxyphilic NbO_x [J]. Applied Energy, 2022, 328: 120199.

[2] PAGANOTTI A, BESSA C V X, SILVA C C S, PEIXOTO E B, DUQUE J G S, SILVA R A G. Effect of the Ni content on the thermal and magnetic properties of Fe−Ni−Co alloys [J]. Materials Chemistry and Physics, 2021, 261: 124215.

[3] HUANG Si-rui, ZHANG Ji-feng, ZHU He-guo. Synergistic strengthening and toughening of eutectic $C_xCoCr_3Fe_5Ni$ high entropy alloy [J]. Transactions of Nonferrous Metals Society of China, 2024, 34: 1204−1213.

[4] YU Wei, CHONG Xiao-yu, GAN Meng-di, WEI Yan, ZHANG Ai-min, HU Chang-yi, FENG Jing. Effect of alloying elements on thermoelastic properties of Pt-based alloys [J]. Transactions of Nonferrous Metals Society of China, 2023, 33: 1851−1861.

[5] LIU Peng, YUAN Xin-yi, DU Yi-zhe, LONG Mu-jun, DUAN Hua-mei, CHEN Deng-fu. Exploration of electrodeposited process of Ni−Co−Cr coating and investigation of Cr doping strengthening mechanism by indentation simulation [J]. Journal of Materials Processing Technology, 2023, 311: 117818.

[6] FARZANEH M A, RAEISSI K, GOLOZAR M A. Effect of current density on deposition process and properties of nanocrystalline Ni−Co−W alloy coatings [J]. Journal of Alloys and Compounds, 2010, 489: 488−492.

[7] KIM J S, KWAK J H, NA S H, LIM S K, SUH S J. The deposit stress behavior and magnetic properties of electrodeposited Ni−Co−Fe ternary alloy films [J]. Journal of the Korean Physical Society, 2012, 61: 609−612.

[8] ZHU Chen-hui, XU Liu-jie, LIU Mei-jun, GUO Ming-yi, WEI Shi-zhong. A review on improving mechanical properties of high entropy alloy: interstitial atom doping [J]. Journal of Materials Research and Technology, 2023, 24: 7832−7851.

[9] JAIN D, ISHEIM D, HUNTER A H, SEIDMAN D N. Multicomponent high-strength low-alloy steel precipitation-strengthened by sub-nanometric Cu precipitates and M_2C carbides [J]. Metallurgical and Materials Transactions A, 2016, 47: 3860−3872.

[10] WANG Zhang-wei, BAKER I. Interstitial strengthening of a f.c.c. FeNiMnAlCr high entropy alloy [J]. Materials Letters, 2016, 180: 153−156.

[11] SHANG Y Y, WU Y, HE J Y, ZHU X Y, LIU S F, HUANG H L, AN K, CHEN Y, JIANG S H, WANG H, LIU X J, LU Z P. Solving the strength-ductility tradeoff in the medium-entropy NiCoCr alloy via interstitial strengthening of carbon [J]. Intermetallics, 2019, 106: 77−87.

[12] CHEN L B, WEI R, TANG K, ZHANG J, JIANG F, HE L, SUN J. Heavy carbon alloyed FCC-structured high entropy alloy with excellent combination of strength and ductility [J]. Materials Science and Engineering: A, 2018, 716: 150−156.

[13] WANG Zhang-wei, BAKER I, GUO Wei, POPLAWSKY J D. The effect of carbon on the microstructures, mechanical properties, and deformation mechanisms of thermo-mechanically treated $Fe_{40.4}Ni_{11.3}Mn_{34.8}Al_{7.5}Cr_6$ high entropy alloys [J]. Acta Materialia, 2017, 126: 346−360.

[14] KRESSE G, JOUBERT D. From ultrasoft pseudopotentials to the projector augmented-wave method [J]. Physical Review B, 1999, 59: 1758−1775.

[15] MONKHORST H J, PACK J D. Special points for Brillouin-zone integrations [J]. Physical Review B, 1976, 13: 5188−5192.

[16] CHE Can-yan, LI Yang, ZHANG Gui-feng, DENG De-wei. Doped amorphous carbon films prepared by liquid phase electrodeposition [J]. Open Journal of Synthesis Theory and Applications, 2014, 3: 5−13.

[17] ANWAR S, KHAN F, ZHANG Y H. Corrosion behaviour of Zn−Ni alloy and Zn−Ni−nano-TiO_2 composite coatings electrodeposited from ammonium citrate baths [J]. Process Safety and Environmental Protection, 2020, 141: 366−379.

[18] TO D T, PARK S H, KIM M J, CHO H-S, MYUNG N V. Effect of solution pH, precursor ratio, agitation and temperature on Ni−Mo and Ni−Mo−O electrodeposits from ammonium citrate baths [J]. Frontiers in Chemistry, 2022, 10: 1010325.

[19] da SILVA G P, de LIMA R N, SANTOS F J N, de MENEZES F P S, MORAIS L P L, da SILVA FILHO L F. Influence of the complexing agent sodium citrate on the chemical composition, surface morphology and corrosion resistance of Ni−Fe electrodeposits [J]. Transactions of the IMF, 2019, 97: 230−236.

[20] ZAKI M Y, NOUNEH K, TOUHAMI M E, BELAKHMIMA R A, GALCA A C, PINTILIE L, ENCULESCU M, BAIBARAC M, TAIBI M. Effect of mixing complexing agents on the properties of electro- deposited CZTS thin films [J]. Optical Materials, 2018, 83: 252−256.

[21] DEAN J A. Lange's Handbook of Chemistry [M]. McGRAW-HILL, INC [J]. 1999.

[22] KARIMZADEH A, ALIOFKHAZRAEI M, WALSH F C. A review of electrodeposited Ni−Co alloy and composite coatings: Microstructure, properties and applications [J]. Surface and Coatings Technology, 2019, 372: 463−498.

[23] DAHMS H, CROLL I M. The anomalous codeposition of

iron-nickel alloys [J]. Journal of the Electrochemical Society, 1965, 112: 771.

[24] YANG Xu, LU Xue-feng, ZHANG Wei, GUO Xin, REN Jun-qiang, XUE Hong-tao, TANG Fu-ling. Preparation and application of nano-Ni−Co alloy [J]. Journal of Nanoparticle Research, 2023, 25(7): 152.

[25] HAGAROVÁ M, JAKUBÉCZYOVÁ D, CERVOVÁ J. Microstructure and properties of electroplated Ni−Co alloy coatings [J]. International Journal of Electrochemical Science, 2015, 10: 9968−9974.

[26] OLIVEIRA J A M, de ALMEIDA A F, CAMPOS A R N, PRASAD S, ALVES J J N, de SANTANA R A C. Effect of current density, temperature and bath pH on properties of Ni−W−Co alloys obtained by electrodeposition [J]. Journal of Alloys and Compounds, 2021, 853: 157104.

[27] RADADI R M A, IBRAHIM M A M. Nickel-cobalt alloy coatings prepared by electrodeposition, Part II: Morphology, structure, microhardness, and electrochemical studies [J]. Korean Journal of Chemical Engineering, 2021, 38: 152−162.

[28] ZAMANI M, AMADEH A, BAGHAL S L. Effect of Co content on electrodeposition mechanism and mechanical properties of electrodeposited Ni−Co alloy [J]. Transactions of Nonferrous Metals Society of China, 2016, 26: 484−491.

[29] JIA Jing-Jing, MENG Mu, ZHANG Zhi-min, YANG Xue, LEI Gen-xing, ZHANG Hong-lei. Effect of deep cryogenic treatment on the microstructure and tensile property of Mg−9Gd−4Y−2Zn−0.5Zr alloy [J]. Journal of Materials Research and Technology, 2022, 16: 74−87.

[30] SKNAR Y E, SKNAR I V, SAVCHUK O O, DANILOV F I. Electrodeposition of NiCo alloy from methansulfonate electrolyte. The role of the electrolyte pH in the anomalous codeposition of nickel and cobalt [J]. Surface and Coatings Technology, 2020, 387: 125542.

[31] FATIMAH S, RAGADHITA R, AL HUSAENI D F, NANDIYANTO A B D. How to calculate crystallite size from x-ray diffraction (XRD) using Scherrer method [J]. ASEAN Journal of Science and Engineering, 2021, 2: 65−76.

[32] KONG J, HACHÉ M J R, TAM J, MCCREA J L, HOWE J, ERB U. On the extrinsic Hall−Petch to inverse Hall−Petch transition in nanocrystalline Ni−Co electrodeposits [J]. Scripta Materialia, 2022, 218: 114799.

[33] JIANG Yi-ming, CHEN Chun-yi, CHANG T M, LUO Xun, YAMANE D, SONE M. Electrodeposition of Ni−Co alloys and their mechanical properties by micro-vickers hardness test [J]. Electrochem, 2021, 2: 1−9.

[34] FIGUEIREDO R B, KAWASAKI M, LANGDON T G. Seventy years of Hall−Petch, ninety years of superplasticity and a generalized approach to the effect of grain size on flow stress [J]. Progress in Materials Science, 2023, 137: 101131.

[35] THEODOSIOU A, SPENCER B F, COUNSELL J, JONES A N. An XPS/UPS study of the surface/near-surface bonding in nuclear grade graphites: A comparison of monatomic and cluster depth-profiling techniques [J]. Applied Surface Science, 2020, 508: 144764.

[36] COOPER A J, WILSON N R, KINLOCH I A, DRYFE R A W. Single stage electrochemical exfoliation method for the production of few-layer graphene via intercalation of tetraalkylammonium cations [J]. Carbon, 2014, 66: 340−350.

[37] BIESINGER M C, PAYNE B P, GROSVENOR A P, LAU L W M, GERSON A R, SMART R S C. Resolving surface chemical states in XPS analysis of first row transition metals, oxides and hydroxides: Cr, Mn, Fe, Co and Ni [J]. Applied Surface Science, 2011, 257: 2717−2730.

[38] WANG Wei-yan, YANG Yun-quan, LUO He-an, LIU Wen-ying. Effect of additive (Co,La) for Ni−Mo−B amorphous catalyst and its hydrodeoxygenation properties [J]. Catalysis Communications, 2010, 11: 803−807.

[39] NESBITT H W, LEGRAND D, BANCROFT G M. Interpretation of Ni 2p XPS spectra of Ni conductors and Ni insulators [J]. Physics and Chemistry of Minerals, 2000, 27: 357−366.

[40] KHASSIN A A, YURIEVA T M, KAICHEV V V, BUKHTIYAROV V I, BUDNEVA A A, PAUKSHTIS E A, PARMON V N. Metal–support interactions in cobalt-aluminum co-precipitated catalysts: XPS and CO adsorption studies [J]. Journal of Molecular Catalysis A: Chemical, 2001, 175: 189−204.

[41] WANG Wei-yan, YANG Yun-quan, LUO He-an, HU Tao, LIU Wen-ying. Amorphous Co−Mo−B catalyst with high activity for the hydrodeoxygenation of bio-oil [J]. Catalysis Communications, 2011, 12: 436−440.

[42] SHANG Cai-yun, AXINTE E, SUN Jun, LI Xu-ting, LI Peng, DU Jian-wei, QIAO Peng-chao, WANG Yan. CoCrFeNi ($W_{1-x}Mo_x$) high-entropy alloy coatings with excellent mechanical properties and corrosion resistance prepared by mechanical alloying and hot pressing sintering [J]. Materials & Design, 2017, 117: 193−202.

[43] MADHAVAN R, BELLON P, AVERBACK R S. Wear resistance of Cu/Ag multilayers: A microscopic study [J]. ACS Applied Materials & Interfaces, 2018, 10: 15288−15297.

[44] WANG Tao, CHEN Long-qing, LIU Zi-kui. Lattice parameters and local lattice distortions in fcc-Ni solutions [J]. Metallurgical and Materials Transactions A, 2007, 38(3): 562−569.

[45] WANG Y, CURTAROLO S, JIANG C, ARROYAVE R, WANG T, CEDER G, CHEN L Q, LIU Z K. Ab initio lattice stability in comparison with CALPHAD lattice stability [J]. Calphad, 2004, 28: 79−90.

[46] KIM D E, SHANG S L, LIU Z K. Effects of alloying elements on elastic properties of Ni_3Al by first-principles calculations [J]. Intermetallics, 2010, 18: 1163−1171.

[47] YANG Zhi-biao, LU Song, TIAN Yan-zhong, GU Zi-jian, MAO Hua-hai, SUN Jian, VITOS L. Assessing the magnetic order dependent γ-surface of Cr−Co−Ni alloys [J]. Journal of Materials Science & Technology, 2021, 80: 66−74.

[48] HU Qing-feng, LIU Yuan, ZHENG Xue-rong, ZHANG Jin-feng, WANG Jia-jun, HAN Xiao-peng, DENG Yi-da, HU Wen-bin. How the surface Cu layer affected the activity of Ni foil for alkaline hydrogen evolution [J]. Journal of Materials Science & Technology, 2024, 169: 11−18.

[49] SILVI B, SAVIN A. Classification of chemical bonds based on topological analysis of electron localization functions [J]. Nature, 1994, 371: 683−686.

Ni−Co−C 合金涂层的合成与性能强化机制

杜一哲[1]，陈桢垚[1]，段华美[1]，龙木军[1,2]，陈登福[1]

1. 重庆大学 材料科学与工程学院 材料与冶金实验室，重庆 400044；
2. 重庆大学 先进铸造技术国家重点实验室，重庆 400044

摘　要：采用电沉积技术在草酸铵−柠檬酸铵体系中制备具有优异综合性能的 Ni−Co−C 合金涂层。优化后的涂层结晶致密，表面呈明显的颗粒状，且大尺寸颗粒表面密集分布着纳米级颗粒团簇。此外，C 原子主要以固溶体形式存在于涂层中，维持涂层原有的 FCC 结构。与二元 Ni−Co 涂层相比，Ni−Co−C 涂层在硬度、耐磨性和结合强度方面都有显著提升，这主要归因于 C 原子的潜在强化作用。C 原子的引入优化了合金的局部电荷密度和电子分布状态，促使局部弱离子键转变为强共价相互作用，增强了 Ni−Co 块体中相应原子之间的成键能力。

关键词：Ni−Co−C 合金涂层；电沉积；耐磨性；电子特性；强化机制

(Edited by Xiang-qun LI)